X-ray microtomography characterisation of the changes in statistical homogeneity of an unsaturated sand during imbibition

J.-F. Bruchon, Jean-Michel Pereira, Matthieu Vandamme, N. Lenoir, Pierre Delage, Michel Bornert

X-ray microtomography characterisation of the changes in statistical homogeneity of an unsaturated sand during imbibition

J.-F. BRUCHON*, J.-M. PEREIRA*, M. VANDAMME*, N. LENOIR*, P. DELAGE* and M. BORNERT*

This paper deals with determination of the size of the representative volume element (RVE) of an unsaturated sand specimen and its evolution during wetting. An imbibition test was conducted in an oedometer cell while stepwise reducing the capillary pressure by using the negative water column technique. X-ray tomography scans were acquired at each equilibrium state and three-dimensional images of a partial volume of the specimen were processed. Characterisation of the sample's homogeneity was based on the asymptotic behaviour method for three quantities of interest: the air fraction and the median diameters of both the air and the water–grain phases obtained from Matheron's granulometry. It is shown that the RVE size depends on the choice of the quantity of interest and evolves with the saturation state.

KEYWORDS: partial saturation; pore pressures; sand; statistical analysis

INTRODUCTION

In soil mechanics, the definition of an objective criterion to evaluate the size of the representative volume element (RVE) and the homogeneity of tested specimens is often addressed because experimental data assume specimen homogeneity. However, due to advanced investigation techniques such as x-ray computed tomography (CT), specimen homogeneity has been qualitatively observed to be questionable in some cases, especially when the specimen is unsaturated, as in the recent studies of Kim *et al.* (2011) and Riedel *et al.* (2012). In the present study, a relatively simple method is proposed to deal with this issue and to assess specimen homogeneity using an imbibition test carried out on a sand specimen.

An imbibition test was conducted in an oedometer cell made up of PMMA (polymethyl methacrylate) specifically designed for x-ray tomography. Capillary pressure in the sample was imposed by using the negative water column technique (Croney, 1952; Fredlund & Rahardjo, 1993; Lins & Schanz, 2005; Vanapalli *et al.*, 2008). The microstructure of the sand was characterised by means of partial CT scans with a 25 μm voxel size in its initial unsaturated state and under several subsequent different hydro-mechanical conditions. Partial CT scans provide local information at a better spatial resolution without the need of reducing the specimen size in order to obtain comparable resolutions.

The microstructural characterisation carried out aimed to quantify the size of the RVE (Matheron & Blondel, 1963; Lantuejoul, 1991; Muir Wood, 2012). The method used was the asymptotic behaviour method (Lantuejoul, 1991; Blanc *et al.*, 2008) applied to the quantities of interest – the air fraction and the median diameter of both the air phase and the water–grain phase (here called the aggregate phase).

*Université Paris-Est, Laboratoire Navier (UMR 8205), CNRS, ENPC, IFSTTAR, Marne-la-Vallée, France

MATERIAL AND METHODS

The specimen comprised loose unsaturated sand composed of Hostun sand HN31 (Flavigny *et al.*, 1990) sieved at 250 μm giving a median grain size of 350 μm. The specimen was prepared by pluviating the sand wetted to a water content $w = 7\%$ and using a shaking table to force water–sand aggregates through two sieves (3·5 and 2·24 mm openings) in order to avoid any hand manipulation of the mixture. Compaction of around 20% was then applied to stabilise the structure. The final state parameters of the compacted specimen were an air fraction $p = 47{\cdot}5\%$, degree of saturation $S_r = 15\%$ and water content $w = 7{\cdot}2\%$. The final specimen was a cylinder of 30 mm height and 70 mm diameter, comparable to a standard oedometer specimen. No vertical stress was applied to the specimen during the imbibition test.

At each imbibition step, a controlled quantity of water was added to the burette and left for at least 4 h to reach equilibrium. The final water level provided both the capillary pressure in the soil and the quantity of water absorbed by the specimen. The highest capillary pressure ($p_c = 7$ kPa) was applied to the compacted specimen at the beginning of the test, leading to some loss of water (step 2 in Fig. 1). Eleven consecutive imbibition steps were then performed to lower the capillary pressure down to zero. At the last step, the meniscus in the burette was at the level of the top of the specimen.

At each equilibrium state, a local CT scan centred on the sample was performed. The reconstructions had a voxel size of 25 μm. A central cube (750^3 voxels (i.e. 18·7 mm side length)) inside these local CT scans (referred to in the following as the 'isolated volume') was extracted and analysed using the freeware Population library (Tariel, 2009) interfaced with the Caméléon graphical language (Cugnon de Sevricourt & Tariel, 2011). A non-linear anisotropic diffusion filter was first applied. A threshold was then used to separate phases. For each image, the first basin of the grey level histogram was used as the threshold value, giving two phases – the air phase and a mixture of sand and water, referred to as the 'aggregate phase' in the following. Such binarisation was preferable to a separation into three phases because of the lack of contrast in images between water and grains. Air attenuation was sufficiently lower than that of the two other phases to isolate the air

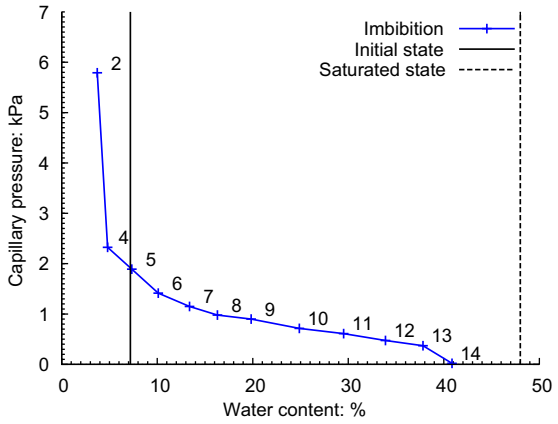

Fig. 1. Capillary pressure at top of specimen as a function of macroscopic water content. The initial state (black solid line) at 7·2% water content and the 'theoretical' saturated state (black dashed line) at 48% are plotted. Each blue cross corresponds to an equilibrium state at which a scan of the specimen was acquired

phase with sufficient accuracy. Owing to the voxel size of 25 µm and the consistently selected spot size of the x-ray tube for the CT scans, the spatial resolution of the images could be evaluated to be noticeably below 50 µm, which is reasonably small compared to the median diameter of the sieved sand (350 µm). Matheron's granulometry (Haas *et al.*, 1967) was applied to both phases with a discrete sphere as the structuring element. Median diameters were computed from cumulative voxel distributions.

The size of the RVE relative to various quantities of interest was investigated by using the asymptotic behaviour method. This method is based on sampling of sub-specimens into the isolated volume. According to Matheron's criterion, homogeneity of the isolated volume is confirmed when the variance of the quantity of interest decreases asymptotically as the inverse of the volume of the sub-specimens. The size of the RVE for a quantity of interest can then be determined as a function of a user-defined level of fluctuation. Three quantities of interests are used in this study – the air fraction and the median diameter of both aggregates and air pores. Note that the analysis presented here was performed on a partial volume of the specimen, the size of which was limited by image artefacts and image resolution. The homogeneity analysis based on this partial volume cannot be readily extrapolated to the whole specimen, in particular if there are heterogeneities in the specimen with a characteristic size greater than that of the partial volume.

RESULTS AND DISCUSSION

Figure 1 shows the capillary pressure at the top of the specimen as a function of macroscopic water content. The vertical lines show the initial state (continuous line) of the specimen and the 'theoretical' saturated state (dotted line) assuming fully saturated porosity in the reference state. Strains increased during imbibition; the macroscopic vertical strain (i.e. the average vertical strain of the whole specimen) reached about 2·5% at step 14, exhibiting sample collapse under self-weight.

The air fraction increased between the initial state and the second step because of the drainage step (Fig. 2(a)). Note that the air fraction at the initial state as evaluated by image processing in the isolated volume (45·3%) is slightly lower than the overall air fraction (47·5%) at the specimen's scale obtained by weighting. The difference might come from image processing uncertainties or/and heterogeneity of the air fraction in the whole specimen. After step 2, the air fraction decreased as a consequence of water infiltration and the median diameters of the two phases (i.e. air and grain–water phases) increased (Fig. 2).

This evolution is illustrated in Fig. 3 where a selected vertical slice of the isolated volume is shown for steps 1, 10 and 14. Visualisation of the three-dimensional (3D) granulometry analysis is also presented for the same slice and at the same steps. Scales are displayed from 0 to 0·6 mm diameter for the air phase (Fig. 3(b)) and from 0 to 2 mm for the aggregate phase (Fig. 3(c)). The figures show the diameter value of the largest inscribed sphere that covers each voxel. Figure 3 confirms that the smallest air-filled pores disappeared during imbibition, leading to an increase in their median diameter, while the water–grain phase grew both in terms of volume fraction and sizes.

Imbibition leads to large variations in terms of air fraction and median diameter of the two phases. In order to quantify the uncertainties associated with these parameters and to assess their homogeneity, RVE size analysis was performed using the asymptotic behaviour method. Figure 4 shows the results for the initial step. The experimental variances were fitted using

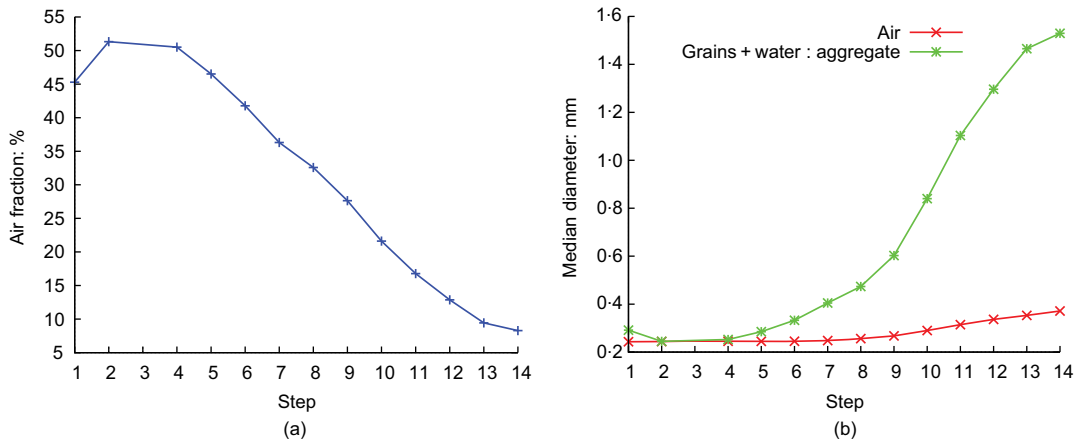

Fig. 2. Air fraction (a) and median diameters of air and water–grain phases (b) obtained by image processing of the isolated volume plotted as a function of wetting step

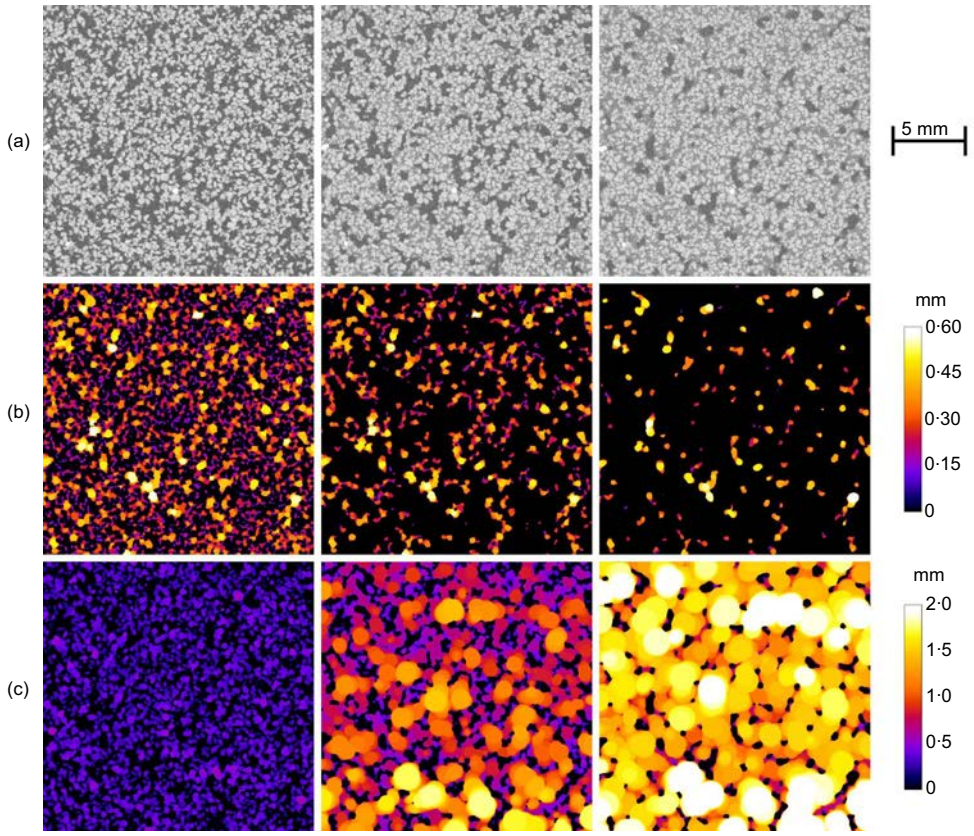

Fig. 3. Maps of a vertical slice of the isolated volume after reconstruction (a), after thresholding and application of Matheron's granulometry on the air phase (b) and on the aggregate phase (c). Colour scales give the value of the diameter of the biggest 3D inscribed spheres (in mm)

$$f(V) = \frac{A\sigma^2}{V^b} \tag{1}$$

where A and b are fitting parameters, σ^2 is the point variance and V is the volume of the sub-specimens. The integral range A allows the characterisation of a typical scale of variation of the quantity under consideration (Lantuejoul, 1991). This corresponds to the abscissa of the intersection point of the dashed line (point variance) and the solid line (equation (1)) (see Fig. 4). The point variance is the variance of the quantity under consideration evaluated on arbitrarily small domains at randomly chosen positions (equal, for instance, to $p(1-p)$ for air fraction p). The integral range has the same dimension as V^b since the point variance σ^2 and f share the same dimension. However, from a theoretical point of view, the integral range has a clear physical meaning (being a volume) only for homogeneous volumes for which parameter b, which defines the decreasing rate of variance, is equal to 1.

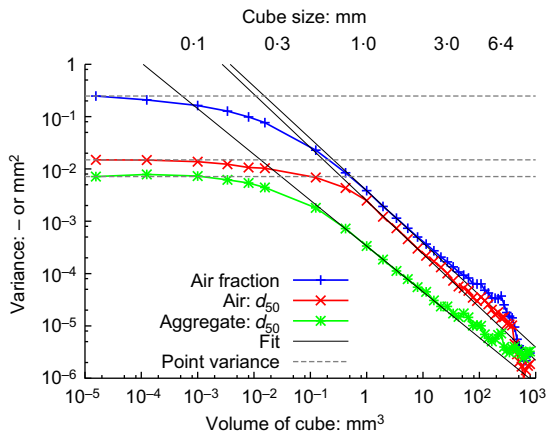

Fig. 4. Variance (dimensionless) of air fraction and variance (in mm^2) of median diameters at the initial state. The dashed lines plot the point variances and solid lines the fits of the variances using equation (1)

When the volume of sub-specimens V tends to zero, the variance tends to the point variance (horizontal dashed lines). The decrease of the variances is then accelerated in the log–log space up to a volume of 1 mm^3 (see Fig. 4). This is typical of the change of scale between microscopic and mesoscopic levels. The mesoscopic homogeneity of the matter appears beyond this volume, and variances become inversely proportional to the volume of the cubic-shaped sub-specimens at the power b. It should be pointed out that the scatter observed at larger volumes is somewhat exaggerated by the log scale. Moreover, the evaluation of the variance is also influenced by the number of sub-samples considered. While we start with 5832 sub-specimens at 1 mm cube size, the scatter seems to start at 3 mm cube size (216 sub-samples) and is enhanced for the last points, for which only eight sub-samples were used, resulting in a higher uncertainty in the evaluation of the variance.

Matheron's criterion states that the specimen is homogenous if $b = 1$, reflecting the idea that the quantities of interest evaluated in disconnected volumes of size V are statistically independent. To be less restrictive, we assume here that an exponent b higher than 0·9 is sufficient to validate the criterion (Fig. 5). At the beginning of the test, the air fraction and median diameter of the air phase satisfy the criterion until step 7, corresponding to an overall water content at sample scale of 13%. The air fraction satisfied this

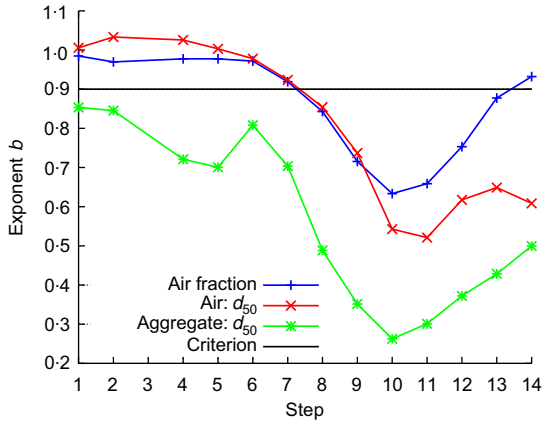

Fig. 5. Exponent b of equation (1) for each quantity of interest and for all steps. The closer b is to 1, the more homogeneous is the sample for the quantity of interest

criterion again at the very last step. However, for all other states and at each state for the aggregate median diameter, the criterion is not verified. So, the median diameter of aggregates was non-uniform within the isolated volume, certainly because of a pronounced heterogeneity of the grain arrangement.

An important result is that the homogeneity of the isolated volume varies over the imbibition process. This result can be explained by the effect of gravity, which leads to a pressure gradient along the height of the specimen. At any equilibrium state, the specimen is characterised by heterogeneity in the water distribution because of the relationship between the water content and the capillary pressure (Fig. 1). Indeed, the difference in water content (Δw) between the bottom and the top of the isolated volume can be approached by equation (2) using the Van Genuchten equation fitted to the w–p_c relationship obtained from the water retention curve of Fig. 1 and the height of the isolated volume ($h_v = 18{\cdot}7$ mm)

$$\Delta w = \frac{\mathrm{d}w}{\mathrm{d}p_c}(p_c)\rho \mathbf{g} h_v \qquad (2)$$

in which $\rho = 1$ Mg/m^3 is the mass density of liquid water, $\boldsymbol{g} = 9{\cdot}81$ m/s^2 is acceleration due to gravity, p_c is the capillary pressure (in Pa) and h_v is in metres. The difference in water content Δw and the level of homogeneity, characterised by exponent b, are strongly linked (Fig. 6): Δw is maximum at

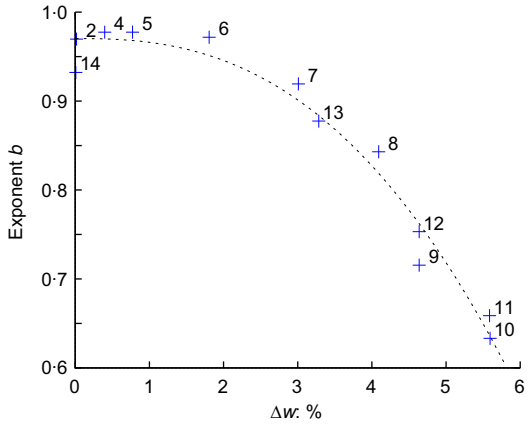

Fig. 6. Exponent b of the air fraction versus the difference in water content between the bottom and top of the isolated volume at each step

step 10 (5·6%) where b is a minimum. Gravity thus has a significant effect on the loss of homogeneity for intermediate saturated states. The height of the specimen therefore affects its mesoscopic behaviour.

The cube root of the integral range of the air fraction and of the median diameter of air (i.e. the side length of a cube that has the same volume) provides the characteristic lengths of these two quantities (Fig. 7). Although the integral ranges for steps 7 to 13 (for the air fraction) and steps 7 to 14 (for the median diameter of air) are meaningless from a theoretical point of view (since the corresponding volume is not homogeneous, $b < 0{\cdot}9$), they have been added to the figure to illustrate the main trend (dashed lines).

The typical scale relative to the air volume fraction turned out to be close to the median diameter of the phases for the first steps (250 μm). In the last step, this characteristic length increased to 450 μm. If the median diameters are weighted by the volume fraction of their complement (black line in Fig. 7), the result is surprisingly close to the cube root of the integral range of the air fraction. This observation suggests that the characteristic length of the air volume fraction depends not only on the size of aggregates or air-filled pores, but also on their relative proportions. In addition, the weighting of the median diameters, which enables approximation of the integral range, shows that this characteristic length is driven by the characteristic length of the phase with the smaller volume fraction (i.e. air-filled pores when most pores are filled with water and water–grain aggregates when most pores are filled with air). It is worth noting that the characteristic lengths depend on the quantity of interest. As an illustration, Fig. 7 also shows the integral range relative to the median diameter of the air phase, which is twice as large as that of the air fraction.

Uncertainties linked to the quantities of interest can be expressed for any volume size if the homogeneity has been proved. For instance, assuming a Gaussian distribution, the 95% confidence interval of the air fraction is $[p - 2\sigma(V); p + 2\sigma(V)]$, which can be rewritten as $p \pm 2\sigma(V)$ with $\sigma^2(V) = f(V)$, f being the function given in equation (1). For instance, with ten mean diameters of the grains (i.e. a cube of 3·5 mm side length), at the first step, 95% of subsamples of this volume size are in the interval $45{\cdot}3 \pm 1{\cdot}9$% for the air fraction and in the interval 243 ± 15 μm for the

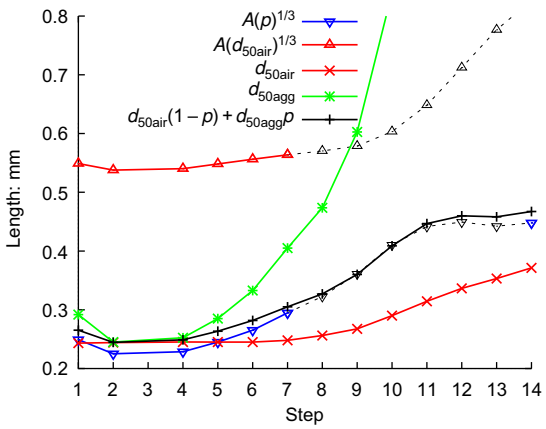

Fig. 7. Median diameter of air and aggregate phases as a function of wetting step. The figure shows the cube root of the air fraction integral range (blue triangles when $b > 0{\cdot}9$ and grey dashed lines when $b < 0{\cdot}9$), the cube root of the integral range of the air median diameter (red triangles) and the sum of the median diameters weighted by the fraction of their complement (black lines with p the air fraction)

median diameter of the air phase. Conversely, if the relative expanded uncertainty ($2\sigma(V)/p$) is limited by 1%, the RVE size can be obtained (see Fig. 8). RVE sizes associated with the median diameter of the air phase and the air fraction calculated with this criterion increased slightly during imbibition until step 7, from about 10 mm to about 15 mm (i.e. around 30 to 45 times the median diameter of the sieved sand). Afterwards, RVE sizes are harder to evaluate since the sample is no longer homogeneous, but seem to reach much larger values when equation (1) is extrapolated with $b \neq 1$. At the last stage of the test when homogeneity is recovered, the RVE size associated with the air fraction turns out to be about 45 mm. This is larger than the size of the isolated volume and has also been obtained by extrapolation of equation (1).

CONCLUSIONS

This study evaluated the homogeneity of 3D images through various quantities of interest (volume fractions and median diameter of phases) during imbibition of unsaturated loose sand. It is concluded that specimen homogeneity depends on the quantity of interest and on the saturation state. A loss of homogeneity was observed for intermediate saturation states. This might be due to the hydrostatic pressure and the water-retaining properties of the material, which led to an overly heterogeneous distribution of water content along the height of the specimen. The RVE size cannot be determined for these states and the specimen response is the result of heterogeneities at the mesoscopic scale. For states where homogeneity is verified, the characteristic length that governs the fluctuations of the air fraction was determined by the median diameters of the air and of the water–grain phases, weighted by the volumetric fraction of their complement. In this case, the characteristic size of the phase with the lower volume fraction controls the characteristic length of the fluctuations of their proportions. However, the main result of this work shows that some macroscopic measurements carried out in laboratory experiments on unsaturated granular materials can carry uncertainties since the experimental data are not based on an RVE in the strict sense. Knowing this, it could be possible to determine these uncertainties in order to evaluate their effects on macroscopic results. Taking into account the effects of gravity will require specific treatments (numerical inverse-analyses for example) to interpret the experimental data obtained at the macroscopic scale.

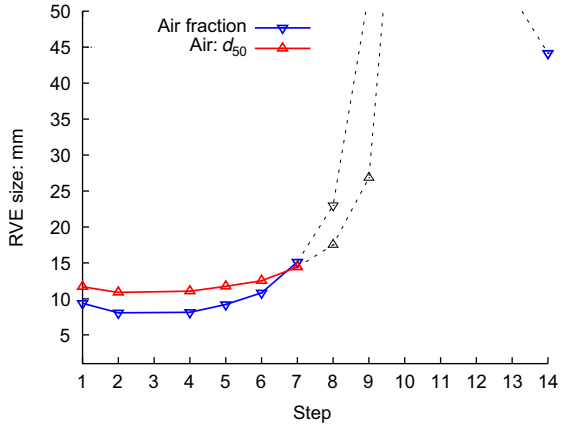

Fig. 8. RVE size of air fraction and of median diameter of air as a function of the considered step. RVE size is the side length of the cube giving a relative expanded uncertainty of 1%. Grey lines correspond to the steps at which the isolated volume was heterogeneous

Acknowledgements

The Laboratoire Navier microtomograph used to run these experiments was acquired with financial support from Région Île-de-France. The authors would like to thank Vincent Tariel for his advice in processing images with the Caméléon–Population software.

REFERENCES

Blanc, R., Da Costa, J., Stitou, Y., Baylou, P. & Germain, C. (2008). Assessment of texture stationarity using the asymptotic behavior of the empirical mean and variance. *Image Process.* **17**, No. 9, 1481–1490.

Cugnon de Sevricourt, O. & Tariel, V. (2011). Caméléon language part 1: Processor. *CoRR* abs/1110.4802. See http://arxiv.org/abs/1110.4802 (accessed 20/05/2013).

Croney, D. (1952). The movement and distribution of water in soil. *Géotechnique* **3**, No. 1, 1–16.

Flavigny, E., Desrues, J. & Palayer, B. (1990). Note technique – le sable d'Hostun 'RF'. *Rev. Française Géotech.* **53**, 67–69.

Fredlund, D. G. & Rahardjo, H. (1993). An overview of unsaturated soil behavior. In *Unsaturated soils* (Houston, S. L. and Wray, W. K. (eds)). Reston, VA: American Society of Civil Engineers, Geotechnical Special Publication, No. 39, pp. 1–31.

Haas, A., Matheron, G. & Serra, J. (1967). Morphologie mathématique et granulométrie en place. *Ann. Mines* **11**, Novembre et Décembre, 736–753.

Kim, F. H., Penumadu, D. & Hussey, D. S. (2011). Water distribution variation in partially saturated granular materials using neutron imaging. *J. Geotech. Geoenviron. Engng* **138**, No. 2, 147–154.

Lantuejoul, C. (1991). Ergodicity and integral range. *J. Microscopy* **161**, No. 3, 387–403.

Lins, Y. & Schanz, T. (2005). Determination of hydro-mechanical properties of sand. *Int. Conf. on Experimental Evidence towards Numerical Modeling of Unsaturated Soils* (T. Schanz (ed.)). New York: Springer, Lecture Notes in Applied Mechanics, pp. 11–29.

Matheron, G. & Blondel, F. (1963). *Traité de géostatistique appliquée*. Paris: Editions Technip.

Muir Wood, D. (2012). Heterogeneity and soil element testing. *Géotech. Lett.* **2**, No. 3, 101–106.

Riedel, I., Andò, E., Salager, S., Bésuelle, P. & Viggiani, G. (2012). Water retention behaviour explored by X-ray CT analysis. *2nd European Conf. on Unsaturated Soils*, Napoli, Italy, pp. 81–88.

Tariel, V. (2009). *Image analysis of cement paste: relation to diffusion transport*. PhD thesis, Ecole Polytechnique, Paris, France.

Vanapalli, S., Nicotera, M. & Sharma, R. (2008). Axis translation and negative water column techniques for suction control. *Geotech. Geol. Engng* **26**, No. 6, 645–660.